Probing the Dependence of Long-Range, Four-Atom Interactions on Intermolecular Orientation. 1. Molecular Hydrogen and Iodine Monochloride

Joshua P. Darr,[†] Andrew C. Crowther,[‡] and Richard A. Loomis*[,§]

Department of Chemistry, Washington University, One Brookings Drive, CB 1134, Saint Louis, Missouri 63130

Sara E. Ray and Anne B. McCoy[§]

Department of Chemistry, The Ohio State University, Columbus, Ohio 43210

Received: August 11, 2007; In Final Form: October 2, 2007

The dependence of the long-range interactions between molecular hydrogen and iodine monochloride on the geometry between the molecules is investigated. Laser-induced fluorescence and action spectroscopy experiments have identified multiple conformers of the *o,p*-$H_2\cdots I^{35,37}Cl(X,v''=0)$ van der Waals complexes. A conformer with the hydrogen molecule localized at the iodine end of the dihalogen, most likely with C_{2v} symmetry, is significantly more stable than an asymmetric conformer with the hydrogen localized in the well oriented orthogonally to the I−Cl bond axis, $D_0'' = 186.4(3)$ cm^{-1} versus $82.8(3) \le D_0'' \le 89.6(3)$ cm^{-1}. Complexes containing the *o*-$H_2(j=1)$ species are more strongly bound than those with *p*-$H_2(j=0)$. The electronically excited *o,p*-$H_2\cdots I^{35}Cl(A,v')$ and *o,p*-$H_2\cdots I^{35,37}Cl(B,v')$ complexes are found to have preferred asymmetric structures with binding energies bracketed between 73.7−80.5 and 69.5−76.3 cm^{-1} for *o*-$H_2\cdots I^{35}Cl(A,v'=23)$ and *o*-$H_2\cdots I^{35}Cl(B,v'=3)$, respectively. Calculations of the $H_2\cdots I^{35}Cl(B,v'=3)$ intermolecular vibrational energies and probability amplitudes undertaken using a scaled He + ICl(B,$v'=3$) potential enable us to make tentative assignments of the excited-state levels experimentally accessed.

1. Introduction

This paper expands on our previous efforts that have focused on characterizing the multidimensional potential energy surfaces (PESs) of ground and excited-state three-atom, rare gas−dihalogen, Rg···XY, van der Waals complexes.[1−6] Here, we present spectroscopic results for the four-atom $H_2\cdots ICl$ complex that reveal information concerning the nature of the dominant long-range interactions and the dependence of these interactions on intermolecular orientation. Four-atom systems present both new opportunities and challenges. For instance, the presence of two diatomic subunits increases the degrees of freedom that must be considered, especially with respect to internal rotational or bending motion. At the same time, having two diatomic subunits also allows us to more thoroughly study the role of electrostatic interactions in this class of van der Waals complexes.

Rovibronic spectra of *ortho*(*o*)-$H_2/D_2\cdots I_2$ and *para*(*p*)-$H_2/D_2\cdots I_2$ complexes recorded in the I_2 B−X region were reported by Kenny et al.[7] In those spectra, they observed two features shifted by ≈15−20 cm^{-1} to higher energy than the corresponding I_2 B−X, $v'-0$ monomer feature; one feature was attributed to transitions of an *o*-$H_2/D_2\cdots I_2$ complex and the other to transitions of a *p*-$H_2/D_2\cdots I_2$ complex. The intensity of the *o*-$H_2\cdots I_2$ feature was approximately 3 times more intense than the *p*-$H_2\cdots I_2$ feature, in accord with the 3:1 relative population of *o*-H_2 to *p*-H_2 expected for a room-temperature sample of hydrogen. An additional feature, shifted by ≈75 cm^{-1} from the monomer feature, was observed and attributed to transitions of the *o*-$H_2/D_2\cdots I_2$ complex to an excited intermolecular vibrational level. On the basis of similarities of the spectral shifts and rotational contours of the $H_2\cdots I_2$ features with those of previously characterized Rg···I_2 systems, the average geometries of the ground-state *o,p*-$H_2/D_2\cdots I_2(X,v''=0)$ complexes were presumed to be similar to the T-shaped Rg···XY structure with the H_2 or D_2 molecules localized in the toroidal well positioned orthogonally to the I−I bond axis. The lowest intermolecular level within each *o,p*-H_2/D_2 + $I_2(B,v')$ excited-state PES was also believed to have a similar geometry. The binding energies for the ground-state *o*-$H_2\cdots I_2(X,v''=0)$ and excited-state *o*-$H_2\cdots I_2(B,v'=28)$ complexes were measured to be 92.3 and 74.4 cm^{-1}, respectively.

If the $H_2\cdots I_2(X,v''=0)$ complexes have on average C_{2v} symmetry, such as

then quadrupole−quadrupole forces would be the dominant electrostatic interaction. In contrast, dipole−quadrupole and dipole−induced dipole dispersion forces will most likely be the dominant electrostatic interactions that dictate the properties of the multidimensional PESs associated with heteronuclear $H_2\cdots XY$ complexes, such as $H_2\cdots ICl$. The somewhat classical use of electrostatic forces in explaining the observed intermolecular interactions is admittedly overly simplistic because the electronic orbitals of the molecules and the partial exchange of charge via donor−acceptor interactions play key roles in dictating preferred geometries of these complexes. However, this picture gives a good first-order approximation of the

[†] Present address: JILA, University of Colorado, Campus Box 440, Boulder, CO 80309, USA.

[‡] Present address: Department of Chemistry, University of Wisconsin−Madison, 1101 University Ave., Madison, WI 53706, USA.

[§] Electronic mail: R.A.L., loomis@wustl.edu; A.B.M., mccoy@chemistry.ohio-state.edu.

10.1021/jp076465u CCC: $37.00
Published on Web 12/04/2007

interactions involved. Consequently, a comparison of the preferred geometries and intermolecular vibrational energies for the $H_2\cdots I_2$ and $H_2\cdots ICl$ complexes should provide insight into the contribution of electrostatic forces in the long-range, intermolecular interactions for these four-atom systems.

We present here the results from laser-induced fluorescence (LIF) and action spectroscopy experiments aimed at characterizing the ground- and excited-state interactions of H_2 with ICl. Discrete rovibronic features associated with transitions of two different ground-state $H_2\cdots ICl(X,v''=0)$ conformers are observed. One conformer most likely has a C_{2v}, near-prolate symmetric top geometry with the H_2 moiety localized at the iodine end of the dihalogen, similar to the structures of the linear $Rg\cdots XY(X,v''=0)$ conformers.[2−4,6,8] The other conformer is most likely asymmetric with the H_2 molecule localized in the toroidal potential well oriented orthogonally to the I−Cl bond axis, similar to the structures of the near T-shaped $Rg\cdots XY(X,v''=0)$ conformers.[2−4,6,8] By performing experiments with a carrier gas consisting of predominantly p-H_2 in He, we have also identified which $H_2\cdots ICl$ features can be associated with transitions of complexes containing either o-H_2 or p-H_2. The binding energy of each ground-state conformer is determined, revealing that the C_{2v} conformer is much more strongly bound than the asymmetric conformer for both the o-$H_2\cdots ICl(X,v''=0)$ and p-$H_2\cdots ICl(X,v''=0)$ complexes. The excited-state o,p-$H_2\cdots ICl(B,v')$ and o,p-$H_2\cdots ICl(A,v')$ complexes are both found to have an average asymmetric geometry in the most strongly bound intermolecular vibrational level with no indication of other minima along the angular coordinate about the dihalogen. These observations are consistent with earlier studies of a variety of $Rg\cdots XY(B,v')$ complexes.[2−4,6,8] To assign the numerous excited-state intermolecular vibrational levels associated with the observed transitions, the energies and probability amplitudes of the bound $H_2\cdots ICl(B,v'=3)$ levels were calculated. Last, comparisons of the energetics and geometries of the o,p-$H_2\cdots ICl$ complex with other $H_2\cdots$diatom systems, including $H_2\cdots HF$,[9] $H_2\cdots HCl$,[10] $H_2\cdots OH$,[11] $H_2\cdots NH$,[12] and $H_2\cdots CN$,[13−15] help to elucidate the role of electrostatic interactions in these four-atom systems.

2. Experimental Section

Ground-state $H_2\cdots ICl(X,v''=0)$ van der Waals complexes were stabilized and laser-induced fluorescence (LIF) and action spectra of the complexes were recorded in a manner similar to that described previously for the He···ICl and Ne···ICl complexes.[1,3,16] As with Ne···ICl, the carrier gas of interest was diluted in He so that the propensity for forming higher order complexes, in this case $(H_2)_m\cdots ICl(X,v''=0)$ with $m \geq 2$, was minimized. Numerous LIF spectra were acquired with systematically varied expansion conditions to optimize the signal-to-noise levels of the $H_2\cdots ICl$ features and to aid in determining spectroscopic assignments of the features. Specifically, by varying the reduced distances downstream at which the spectra were recorded, $Z = x/d$, where x is the downstream distance and d is the nozzle diameter, 0.89(3) mm, we characterized the dependence of the intensities of each $H_2\cdots$ ICl feature on the local temperature within the expansion. The local rotational temperature associated with the conditions utilized when acquiring the spectra was determined by recording an LIF spectrum of the $I^{35}Cl$ B−X, 2−0 monomer band and fitting the rotational contour assuming a Boltzmann-rotational distribution. The H_2/He backing pressure and the concentration of H_2 in He were also varied to determine the effects of varying the H_2/ICl and $H_2/H_2\cdots ICl$ collision frequency on the formation of different ground-state conformers. The optimum conditions for recording LIF spectra of the $H_2\cdots ICl$ complexes in both the ICl B−X and A−X regions were obtained when a carrier-gas mixture of 5% H_2 in He was used with a 7.9 bar backing pressure and the laser crossing the expansion at $Z \approx 11$. Unless explicitly stated otherwise, these conditions were used in acquiring the presented spectra. The $I^{35}Cl(X,v''=0)$ rotational temperature determined when these conditions were used was typically ≈1.8 K.

High-purity p-$H_2(j=0)$ in He was used as a carrier gas in some experiments to assist in distinguishing the p-$H_2\cdots ICl$ features from the o-$H_2\cdots ICl$ features. The p-H_2 was prepared in the McCall laboratory in the Chemistry Department at the University of Illinois, Urbana−Champaign, by cooling *normal*(n)-$H_2(j=$even,odd) in liquid He in the presence of a metal catalyst. The resulting p-$H_2(j=0)$ was collected and then diluted with He to an ≈5% concentration. A small fraction of the p-H_2, <10% of the H_2 in the carrier-gas mixture, was observed to convert back into o-$H_2(j=1)$ with increasing storage time in the stainless steel storage cylinder. Nevertheless, significant changes in the relative intensities of the p-$H_2\cdots ICl$ and o-$H_2\cdots ICl$ features were easily recognized when comparing spectra acquired with nearly pure p-H_2/He to those acquired with n-H_2/He.

The LIF experiments were performed using a Nd:YAG-pumped dye laser with a frequency resolution of 0.06 cm^{-1} and typical pulse energies of ≈15 mJ measured within the chamber after being spatially filtered to a diameter of 2−3 mm. The action spectroscopy experiments were performed using an additional Nd:YAG-pumped dye laser system with a frequency resolution of 0.07 cm^{-1}. Pulse energies of the probe laser were maintained at ≈100 μJ when the relatively intense $I^{35}Cl$ E−B, 11−2 and $I^{35}Cl$ β−A, $v^{\dagger}-v'$ transitions were probed, and at ≈500 μJ when the weaker $I^{35}Cl$ E−B, 10−1 transition was probed, to minimize saturation and broadening of the spectral lines. Some spectra were recorded with even higher pump and probe laser intensities to verify that no other weaker spectral features were present in each of the spectral regions. The action spectroscopy experiments were performed with the excitation laser scanning in frequency through the ICl A−X, $v'-0$ or B−X, $v'-0$ region and detecting fluorescence induced by the probe laser from either the ICl(E) or ICl(β) ion-pair states. The pump and probe lasers were co-propagated through the vacuum chamber *via* a dichroic beamsplitter, and the temporal delay of the probe laser pulse from the pump pulse was fixed between 15−20 ns.

3. Theoretical Section

To complement the experimental findings, we performed calculations of the $H_2\cdots I^{35}Cl$ intermolecular vibrational energies within the H_2 + ICl(B,$v'=3$) PES, using a model potential based on the He + ICl(B,$v'=3$) surface. On the basis of the weak interaction between H_2 and ICl, we assume that there is little dependence on the orientation of the H_2 axis relative to the ICl moiety and treat it as spherical, behaving similarly to He, but with a mass of 2.015 650 amu. In addition, our recent studies of He···ICl,[2,17] He···Br_2,[4] and He···I_2[6] indicate that the rovibronic spectra are relatively insensitive to the details of the B-electronic-state surface so long as the minimum is reasonably well described and the potential barriers at the linear and antilinear regions occur at approximately the correct energy. We elected to start with the adiabatic He + ICl(B,$v'=3$) potential, on the basis of the parameters of Waterland and Lester,[18] and scale it to provide reasonable agreement for the energies of the

$H_2\cdots$ICl(B,v'=3) intermolecular vibrational levels. This was achieved through the following expression written in terms of wavenumbers, where we have chosen the zero in energy to correspond to the energy of fully dissociated H_2 + ICl(B,v'=3) and He + ICl(B,v'=3):

$$V_{H_2\cdots ICl}(R,\theta) = 4V_{He\cdots ICl}(R,\theta) - 75\ cm^{-1}$$

In our expression of the potential, R represents the center-of-mass separation of ICl and H_2 and ICl and He, and θ provides the angle between R and the ICl bond axis with $\theta = 0°$ corresponding to the iodine end of ICl. The factor of 4 and the offset of -75 cm^{-1} resulted in the best overall agreement between the calculated and observed energy levels. As an independent check, we also compared the calculated frequencies to those measured for $D_2\cdots$ICl(B,v'=3).[19]

The potential was used to calculate the $H_2\cdots I^{35}$Cl(B,v'=3) intermolecular vibrational levels in the same manner as in earlier studies on He$\cdots$XY systems.[2,4,6,17] The two-dimensional system was solved in a DVR with 120 points in R, evenly spaced between 2 and 26 Å and 30 points in θ that are based on a Gauss−Legendre quadrature grid. Tests with different basis set sizes and ranges in R indicate that the levels that are bound by at least 7.5 cm^{-1} are converged to better than 0.5 cm^{-1}. The Hamiltonian for these calculations is given by

$$\hat{H} = -\frac{\hbar^2}{2\mu_r}\frac{\partial^2}{\partial r^2} - \frac{\hbar^2}{2\mu_R}\frac{\partial^2}{\partial R^2} + \frac{j^2}{2\mu_r r^2} + \frac{l^2}{2\mu_R R^2} + V(r,R,\theta)$$

The mass associated with R is the reduced mass of the complex μ_R, and the reduced mass of I^{35}Cl with a vibrationally averaged bond length r is μ_r. The rotational angular momentum of the ICl molecule in a space-fixed coordinate system is j. The angular momentum associated with the rotation of R in a complex-fixed coordinate system in which the z-axis is defined to lie along the ICl bond is l.

In addition to two-dimensional calculations, we also performed adiabatic calculations, averaging the two-dimensional potential over the two lowest energy eigenstates in $\boldsymbol{R}$ as a function of θ. Once these potentials are evaluated, one-dimensional calculations of the bending levels are performed. Results of both calculations are presented in section 4E.

4. Results

A. $H_2\cdots$ICl LIF and Action Spectra. The LIF spectrum recorded in the ICl B−X, 2−0 and 3−0 regions using a 5% n-H_2/He carrier gas contains multiple discrete features attributed to transitions of $I^{35,37}$Cl molecules and of He$\cdots I^{35,37}$Cl and $H_2\cdots I^{35,37}$Cl complexes, Figure 1a. The $I^{35,37}$Cl features are labeled with asterisks. The features attributed to transitions of the T-shaped and linear He$\cdots I^{35,37}$Cl(X,v''=0) complexes to intermolecular vibrational levels within the He + ICl(B,v'=2,3) potentials have been thoroughly characterized[1,2,16,20,21] and are marked with daggers in the figure. We assign the remaining discrete features to transitions of o,p-$H_2\cdots I^{35,37}$Cl(X,v''=0) complexes to metastable intermolecular vibrational levels within the H_2(j=0,1) + ICl(B,v'=2,3) potentials.

Two-laser, action spectroscopy experiments were performed in the same spectral region to assist in assigning the transitions associated with the $H_2\cdots I^{35,37}$Cl features observed in the LIF spectrum. The action spectra are simplified in comparison to the LIF spectra for two main reasons. First, a spectrum can be recorded that contains only those features associated with transitions of complexes containing either the I^{35}Cl or the I^{37}Cl isotopomer because the probe laser is fixed on an I^{35}Cl or I^{37}Cl E−B, $v^{\dagger}-v'$ transition, which are at distinctly different energies. Second, we can take advantage of the vibrational predissociation dynamics of the complexes occurring in the excited state to identify those features associated with transitions to intermolecular vibrational levels lying within the same excited-state potential. Weakly bound complexes in the excited state undergo vibrational predissociation forming products predominantly in the highest energetically accessible channel. Therefore, spectra containing those features associated with transitions of either He$\cdots I^{35}$Cl(X,v''=0) or $H_2\cdots I^{35}$Cl(X,v''=0) complexes to intermolecular vibrational levels lying within the He + I^{35}Cl(B,v'=2) or H_2 + I^{35}Cl(B,v'=2) PESs can be recorded preferentially by fixing the probe laser on the I^{35}Cl E−B, 10−1 transition and scanning the pump laser through the ICl B−X region. Transitions of the I^{35}Cl monomer can also be observed in this action spectrum because collisions between carrier gas atoms or molecules with excited-state I^{35}Cl(B,v'=2) molecules may result in vibrational relaxation of the dihalogen, which would result in population of rotor states in the I^{35}Cl(B,v'=1) level. The vibrational predissociation of some complexes, such as Ne$\cdots$ Cl_2(B,v'),[22] has been observed to populate a distribution of Cl_2-(B,v) product levels, spanning from the highest energetically available product level down to rotational states with two or three fewer vibrational quanta. We have thus recorded action spectra throughout multiple vibronic regions and with the laser fixed on the I^{35}Cl E−B, 10−1 or 11−2 band heads to identify

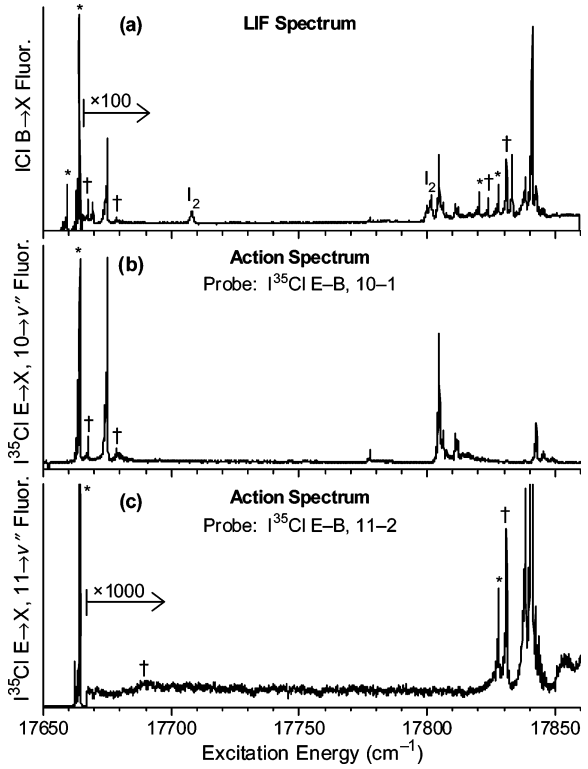

Figure 1. Laser-induced fluorescence (LIF) and action spectra acquired in the ICl B−X, 2−0 and 3−0 spectral region. The LIF spectrum (a) is dominated by the intense $I^{35,37}$Cl B−X, 2−0 transitions at lower energies. Features associated with transitions of the T-shaped and linear He$\cdots I^{35,37}$Cl(X,v''=0) complexes and the $H_2\cdots I^{35,37}$Cl(X,v''=0) complexes are observed to higher energy and are ≈100 times weaker. The action spectra in panels b and c were recorded by probing the I^{35}Cl E−B, 10−1 transition, the $\Delta v = -1$ channel, and the I^{35}Cl E−B, 11−2 transition, the $\Delta v = 0$ channel, respectively. Note the scale change in panels a and c. The bare $I^{35,37}$Cl and He$\cdots I^{35,37}$Cl transitions are marked by asterisks and daggers, respectively. Trace I_2 contamination was also observed in the LIF spectrum and is identified.

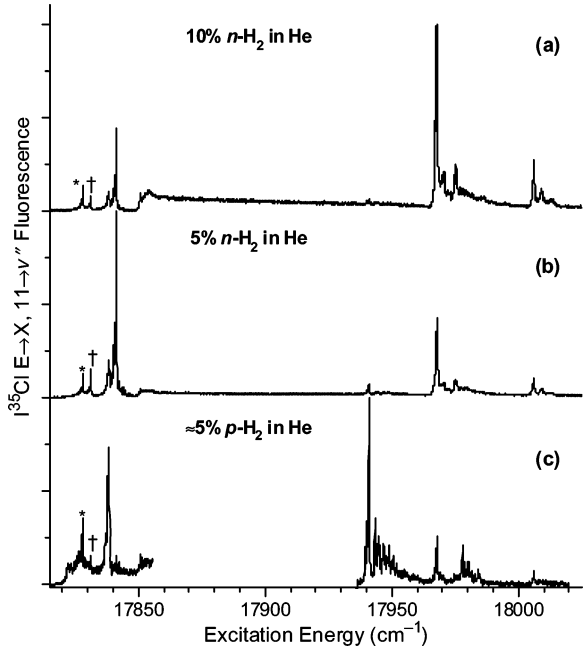

Figure 2. Action spectra recorded in and above the ICl B−X, 3−0 region using different source conditions. The top and middle traces were acquired with a 10% and 5% *n*-H_2 in He carrier gas, respectively. The bottom traces were acquired using a 5% *p*-H_2 in He carrier gas. Note the drastic change in the relative intensities of the features with the change in the carrier gas. The bare $I^{35}Cl$ and He···$I^{35}Cl$ transitions are marked by asterisks and daggers.

those features that access levels in the same excited-state potential.

An action spectrum recorded with the probe laser fixed on the $I^{35}Cl$ E−B, 10−1 transition, and using the same source conditions as the LIF spectrum in Figure 1a is shown in Figure 1b. The $I^{35}Cl$ and He···$I^{35}Cl$ features are marked with asterisks and daggers, respectively. At least five prominent features attributed to transitions of *o*,*p*-H_2···$I^{35}Cl$ complexes are observed in Figure 1b that are also observed in the LIF spectrum. The most intense feature is observed at 17 675 cm^{-1}, ≈11 cm^{-1} above the $I^{35}Cl$ B−X, 2−0 band origin. The other four features are positioned more closely to the $I^{35}Cl$ B−X, 3−0 band origin, at 17 827 cm^{-1}, with peak intensities at 17 778, 17 805, 17 811, and 17 843 cm^{-1} or shifts of ≈114, 141, 147, and 179 cm^{-1} from the $I^{35}Cl$ B−X, 2−0 band origin. A similar action spectrum was recorded with the probe laser fixed on the $I^{35}Cl$ E−B, 11−2 transition and scanning from 17 660 through to 18 100 cm^{-1}, Figure 1c. The discrete H_2···$I^{35}Cl$ features observed in Figure 1b are not observed. The very intense features at 17 838 and 17 841 cm^{-1}, with the latter feature extending off the vertical scale in Figure 1c, are also present in the LIF spectrum, Figure 1a but are not present in Figure 1b. Continuum signals with discrete onsets at 17 850.5 and 17 820.9 cm^{-1} are also observed in the action spectrum, and these signals are associated with bound-free transitions of H_2···$I^{35}Cl(X,v''=0)$ complexes to the continuum of states above the $H_2 + I^{35}Cl(B,v'=2)$ dissociation limit, as discussed in section 4D.

A progression of H_2···$I^{35}Cl$ features is observed to even higher energies in the action spectrum recorded with the probe laser fixed on the $I^{35}Cl$ E−B, 11−2 band head, Figure 2b. In this spectrum, there are two features observed to just higher transition energies than the $I^{35}Cl$ B−X, 3−0 band origin, at 17 827 cm^{-1}. When a 5% *n*-H_2/He carrier gas at a backing pressure of 7.9 bar is used, the slightly higher energy feature at 17 841.21 cm^{-1} is ≈5× more intense than the lower energy feature at 17 838.37 cm^{-1}. At least four additional features are observed to significantly higher transition energies, at ≈17 941, 17 968, 17 975, and 18 006 cm^{-1}, with relative intensities similar to those observed in Figure 1b. Other than the feature at 17 841.21 cm^{-1} with a shift of 14 cm^{-1} from the $I^{35}Cl$ B−X, 3−0 monomer band origin, the energy shifts of the other four discrete features, 114, 141, 148, and 179 cm^{-1}, are nearly identical to the shifts of the discrete features observed in the $I^{35}Cl$ B−X, 2−0 region. The transition energies of the peak intensities of the *o*-H_2···ICl and *p*-H_2···ICl features in both the ICl B−X, 2−0 and 3−0 regions are listed in Table 1. The similar energy shifts of the H_2···$I^{35}Cl$ features from the corresponding $I^{35}Cl$ monomer band origins suggest that the discrete features observed in each action spectrum can be attributed to transitions of H_2···$I^{35}Cl(X,v''=0)$ complexes to the same set of intermolecular vibrational levels lying within the $H_2 + I^{35}Cl(B,v'=2)$ and $H_2 + I^{35}Cl(B,v'=3)$ PESs, respectively. The H_2···$I^{35}Cl$ complexes promoted to these intermolecular levels undergo vibrational predissociation forming products predominantly in the $\Delta v = -1$ channels, $H_2 + I^{35}Cl(B,v'=1)$ and $H_2 + I^{35}Cl(B,v'=2)$, that are detected by the probe laser when recording each action spectrum.

Both LIF and action spectra were also recorded in the ICl A−X, $v'-0$ spectral regions with $v' = 20-25$. Due to the closely spaced ICl energy levels, the spectral congestion in this region makes assignments difficult, especially for the higher energy features. Additionally, the features are significantly broadened, presumably from prompt vibrational predissociation. Nevertheless, in each vibrational region the spectra look similar to those shown in Figures 1 and 2. There are a couple of discrete H_2···ICl features just to higher energy than the monomer band origin and additional features to significantly higher transition energies.

TABLE 1: Transition Energies and Shifts from the $I^{35}Cl$ B−X, 2−0 and 3−0 Monomer Band Origins (cm^{-1}) of the Peaks of the Observed H_2···$I^{35}Cl$ Features[a]

peak	shift	assignment 2−0	peak	shift	assignment 3−0
17 664.1	0.0	$I^{35}Cl$	17 827.5	0.0	$I^{35}Cl$
17 674.9	10.8	asymmetric *o*,*p*-H_2···$I^{35}Cl$	17 838.2	10.7	asymmetric *p*-H_2···$I^{35}Cl$
			17 841.1	13.6	asymmetric *o*-H_2···$I^{35}Cl$
17 777.7	113.6	C_{2v} *p*-H_2···$I^{35}Cl$	17 941.0	113.5	C_{2v} *p*-H_2···$I^{35}Cl$
			17 943.3	115.8	C_{2v} *p*-H_2···$I^{35}Cl$
			17 944.7	117.2	C_{2v} *p*-H_2···$I^{35}Cl$
			17 946.8	119.3	C_{2v} *p*-H_2···$I^{35}Cl$
			17 948.8	121.3	C_{2v} *p*-H_2···$I^{35}Cl$
			17 950.5	123.0	C_{2v} *p*-H_2···$I^{35}Cl$
			17 951.9	124.4	C_{2v} *p*-H_2···$I^{35}Cl$
			17 955.1	127.6	C_{2v} *p*-H_2···$I^{35}Cl$
			17 958.5	131.0	C_{2v} *p*-H_2···$I^{35}Cl$
17 804.8	140.7	C_{2v} *o*-H_2···$I^{35}Cl$	17 967.8	140.3	C_{2v} *o*-H_2···$I^{35}Cl$
17 806.3	142.2	C_{2v} *o*-H_2···$I^{35}Cl$	17 970.1	142.6	C_{2v} *o*-H_2···$I^{35}Cl$
17 807.7	143.6	C_{2v} *o*-H_2···$I^{35}Cl$	17 972.5	145.0	C_{2v} *o*-H_2···$I^{35}Cl$
17 810.9	146.8	C_{2v} *o*-H_2···$I^{35}Cl$	17 974.7	147.2	C_{2v} *p*-H_2···$I^{35}Cl$
17 813.7	149.6	C_{2v} *o*-H_2···$I^{35}Cl$	17 975.2	147.7	C_{2v} *o*-H_2···$I^{35}Cl$
17 816.5	152.4	C_{2v} *o*-H_2···$I^{35}Cl$	17 977.2	149.7	C_{2v} *o*-H_2···$I^{35}Cl$
			17 977.9	150.4	C_{2v} *p*-H_2···$I^{35}Cl$
			17 979.4	151.9	C_{2v} *o*-H_2···$I^{35}Cl$
			17 980.2	152.7	C_{2v} *p*-H_2···$I^{35}Cl$
			17 981.6	154.1	C_{2v} *p*-H_2···$I^{35}Cl$
			17 983.9	156.4	C_{2v} *p*-H_2···$I^{35}Cl$
17 842.7	178.6	C_{2v} *o*-H_2···$I^{35}Cl$	18 006.0	178.5	C_{2v} *o*-H_2···$I^{35}Cl$
17 845.7	181.6	C_{2v} *o*-H_2···$I^{35}Cl$	18 008.9	181.4	C_{2v} *o*-H_2···$I^{35}Cl$
17 848.9	184.8	C_{2v} *o*-H_2···$I^{35}Cl$	18 013.4	185.9	C_{2v} *o*-H_2···$I^{35}Ct$

[a] The assignments correspond to the ground-state conformers associated with the features. Spectra acquired with a carrier gas consisting of high-purity *p*-H_2 in He were only recorded in the ICl B−X, 3−0 region.

B. Signal Dependence upon Source Conditions. We recently reported that the relative populations of the ground-state conformers of rare gas−dihalogen complexes can be changed by varying the source conditions used to form the supersonic expansion in which the complexes are stabilized.[3−6,16] In a similar manner, we have varied the source conditions to track the changing relative intensities of the $H_2\cdots I^{35}Cl$ features to identify those features that can be attributed to transitions of common ground-state complexes. The three parameters varied are the downstream distance at which the spectra were recorded, the H_2/He carrier gas concentration, and the H_2/He backing pressure dependence.

Pronounced changes in the relative intensities of the $H_2\cdots I^{35}Cl$ features are observed in the LIF and action spectra recorded with different H_2/He carrier gas concentrations. The action spectrum recorded throughout the ICl B−X, 3−0 region using a 5% H_2/He carrier gas is plotted in Figure 2b. For this spectrum, the probe laser was fixed on the $I^{35}Cl$ E−B, 11−2 transition, the backing pressure was 7.9 bar and Z was ≈11. The action spectrum plotted in Figure 2a was recorded in the same spectral region and with nearly the same expansion conditions, the only difference being that a 10% H_2/He carrier gas was implemented rather than a 5% mixture. The intensities of the features at significantly higher energy than the $I^{35}Cl$ B−X, 3−0 band origin, at 17 968, 17 975, and 18 006 cm^{-1}, increase relative to those of the features closer to the band origin, at ≈17 838 and 17 841 cm^{-1}, with the increased H_2 concentration. Specifically, the feature at 17 841 cm^{-1} is approximately a factor of 2 more intense than the most intense higher energy feature, at 17 968 cm^{-1}, in Figure 2b. In contrast, the 17 968 cm^{-1} feature is a factor of 2 more intense than the 17 841 cm^{-1} feature when 10% H_2/He is used, Figure 2a. The intensity of the continuum signal observed in the action spectra that has a distinct turn-on at 17 850.5 cm^{-1} is observed to track with the intensity of the higher energy features as the H_2 concentration is varied.

In spectra recorded at varying downstream distances and with varying H_2/He backing pressures, the intensities of the three highest-energy features, at ≈17 968, 17 975, and 18 006 cm^{-1}, are observed to track together, gaining intensity relative to the others with increased distances downstream and with higher H_2/He backing pressures. This suggests that these features are most likely attributable to transitions from the same ground-state $H_2\cdots I^{35}Cl(X,v''=0)$ conformer; furthermore, this conformer is more strongly bound. The intensity of the weakest feature in the higher energy region, at ≈17 941 cm^{-1}, scales approximately with that of the lowest energy feature in this spectral region, at ≈17 838 cm^{-1}, as the gas concentration is varied. The intensity of the 17 941 cm^{-1} feature, however, does not track with that of the 17 838 cm^{-1} feature as the downstream distance is varied. In contrast, it scales much more closely with the intensity of the feature at ≈17 968 cm^{-1} in the distance-dependence spectra. Because these spectra were recorded using a n-H_2/He carrier gas, these complicated trends may be due to exchange of p-H_2 and o-H_2 in the complexes.

Spectra were also acquired with high-purity p-H_2 diluted in He to form a 5% p-H_2/He carrier gas to identify those $H_2\cdots I^{35}Cl$ features associated with o-H_2 and p-H_2 containing complexes. An action spectrum recorded using the same conditions implemented when recording the spectrum in Figure 2b, although with the 5% p-H_2/He carrier gas, is shown in Figure 2c. A set of features gains intensity relative to the other features when the p-H_2/He carrier gas mixture is used in comparison to the intensities of the features in the spectrum acquired with the n-H_2/He mixture. For instance, the discrete features at 17 838 and 17 941 cm^{-1}, which are barely observed in panel b, become the dominant features in panel c. Similarly, a feature is now present at 17 978 cm^{-1} in panel c that is not observable within the signal-to-noise level in the spectra recorded with n-H_2/He, panels a and b. In contrast, the most intense feature in the n-H_2/He spectrum, at 17 841 cm^{-1}, is barely discernible when the p-H_2/He mixture is used. Finally, the weak continuum signal with a turn-on at 17 820.9 cm^{-1} becomes significantly more intense in the p-H_2/He spectrum.

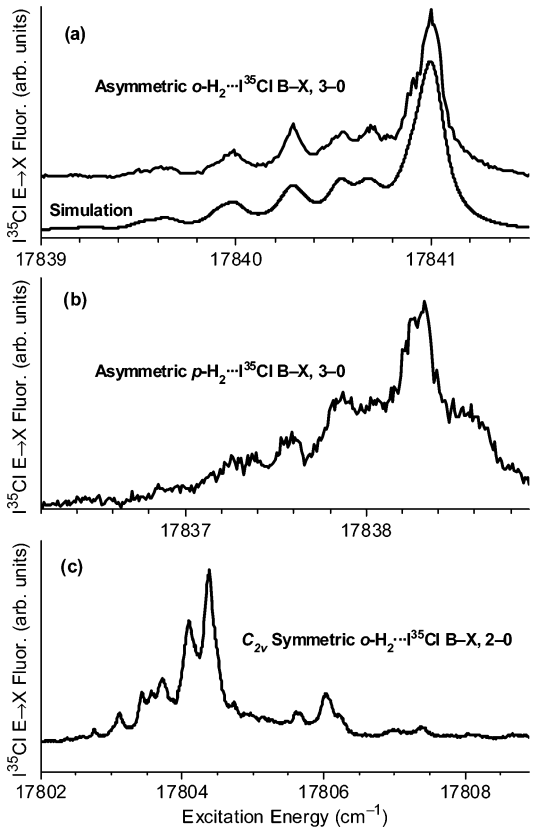

Figure 3. Rotational contour of the lower energy o-$H_2\cdots I^{35}Cl$ B−X, 3−0 feature and the corresponding rigid-rotor fit (a). The rotor constants determined imply a geometry where the H_2 subunit is localized in a well orthogonal to the I−Cl bond axis in both the ground and excited states. We therefore refer to this ground-state o-$H_2\cdots ICl(X,v''=0)$ conformer as asymmetric. The rotational contour of the p-$H_2\cdots I^{35}Cl$ feature observed to just lower energy (b) could not be fit, but similarities in the overall structures of the contours suggest similar average geometries. The rotational contour of the higher energy o-$H_2\cdots I^{35}Cl$ B−X, 2−0 feature (c) could not be fit using a rigid-rotor model. Simulations had significantly fewer lines, suggesting that transitions to multiple intermolecular levels may be overlapping.

The significantly different intensities of the features observed in these action spectra enable us to identify which features are associated with transitions of o-$H_2\cdots I^{35}Cl$ complexes and which are associated with p-$H_2\cdots I^{35}Cl$ complexes. The discrete features observed in the ICl B−X, 3−0 region with transition energies at 17 838, 17 941, and 17 978 cm^{-1} as well as the continuum signal with a turn on at 17 820.9 cm^{-1} are attributed to transitions of p-$H_2\cdots I^{35}Cl$ complexes. The remainder of the features in this spectral region, which dominate the spectra acquired using the n-H_2/He carrier gas, are ascribed to transitions of o-$H_2\cdots I^{35}Cl$ complexes.

C. Geometries of the $H_2\cdots I^{35}Cl$ Conformers. The rotational contour of the lower energy o-$H_2\cdots I^{35}Cl$ feature observed at 17 841 cm^{-1} in the ICl B−X, 3−0 spectral region, Figure 3a, appears quite similar to that of the T-shaped $He\cdots I^{35}Cl$ feature in the 3−0 region.[1] A rigid-rotor model and a genetic learning

algorithm program, *jb95*, developed by D. F. Plusquellic[23] was used to fit the rotational contour of this feature. The rotational contours of the best-fit spectrum and the experimental data are in nearly quantitative agreement, with only minor discrepancies in the intensities of a few rotational lines observed. The ground-state rotational temperature determined in the fit is ≈1.2 K, which is approximately the same as the $I^{35}Cl(X,v''=0)$ ground-state rotational temperature typically measured when these experimental conditions are used. The rotational constants for both the ground-state *o*-$H_2\cdots I^{35}Cl(X,v''=0)$ complex and the excited-state *o*-$H_2\cdots I^{35}Cl(B,v'=3)$ level accessed by this transition, Table 2, are indicative of an average geometry with the center of mass of the H_2 moiety positioned orthogonally to the I−Cl bond axis for both the ground- and excited-state levels. The precise orientation of the H−H bond relative to the ICl moiety, however, remains unknown. Consequently, we will refer to intermolecular levels with this geometry as an asymmetric $H_2\cdots$ICl complex.

The weaker *p*-$H_2\cdots I^{35}Cl$ feature observed at 17 838 cm^{-1} in Figure 2b has a rotational contour similar to that of the *o*-$H_2\cdots I^{35}Cl$ feature at 17 841 cm^{-1}. We attempted to fit the rotational contour of this feature, Figure 3b, in the same manner, and we were not able to obtain an acceptable fit. Specifically, we were not able to reproduce the high-energy shoulder near 17 838.6 cm^{-1}, and the lower signal-to-noise of this feature made it difficult to consistently obtain the same converged parameters. On the basis of the similarities in transition energies and the overall shape of this rotational contour with that of the *o*-$H_2\cdots I^{35}Cl$ feature, we assign this feature to transitions of the asymmetric *p*-$H_2\cdots ICl(X,v''=0)$ complex to an excited-state level with a similar geometry lying within the *p*-H_2 + $I^{35}Cl(B,v'=3)$ intermolecular PES.

The rotational contours of the higher energy features are even more complicated, and we were not able to fit these spectra. A higher energy LIF feature associated with the ICl B−X, 2−0 region is plotted in Figure 3c. In all attempts to fit the rotational contour, an insufficient number of rotational lines were obtained in the simulation. As discussed in section 4E., it is likely that some of the congestion may be due to the presence of several overlapping intermolecular vibrational bands in this region. Additionally, the calculations of the $H_2\cdots I^{35}Cl(B,v'=3)$ probability amplitudes, obtained using the He + ICl(B,v'=3) model potential, indicate that the excited-state levels are delocalized in the angular coordinate about ICl, and thus there is expected to be extensive coupling between the ICl hindered rotation and the end-over-end rotation of the complex. Therefore, the use of a rigid-rotor model to incorporate a fixed geometry within the complex is not appropriate. However, on the basis of comparisons with the spectra of the rare gas−dihalogen complexes, we expect that the ground-state complexes associated with these transitions have geometries with the H_2 moiety localized in the linear well with respect to the I−Cl molecular axis, most likely with C_{2v} symmetry. The geometries of the ground-state conformers associated with each feature are indicated in Table 1.

D. Binding Energies of the $H_2\cdots I^{35}Cl$ Complexes. In the action spectrum recorded with the probe laser fixed on the $I^{35}Cl$ E−B, 11−2 transition, Figures 1c and 2c, continuum signals with discrete onsets at 17 684, 17 850.5, and 17 820.9 cm^{-1} are observed in addition to the discrete features. The weak continuum signal beginning at 17 684 cm^{-1} was observed previously and is attributed to bound to free transitions of the linear $He\cdots I^{35}Cl(X,v''=0)$ complex to the continuum of states lying just above the He + $I^{35}Cl(B,v'=2)$ dissociation limit.[8,24] Similar, bound-free continuum signals were also observed in action spectra of the $Ne\cdots I^{35}Cl$,[3] $He\cdots {}^{79}Br_2$,[4] $Ar\cdots I_2$,[5] and $He\cdots I_2$[6] complexes. Because the continuum signal with a turn-on at 17 850.5 cm^{-1} is only observed with appreciable intensity when the *n*-H_2/He carrier gas is used, this signal is attributed to transitions of *o*-$H_2\cdots I^{35}Cl(X,v''=0)$ complexes to the continuum of states lying just above the *o*-H_2 + $I^{35}Cl(B,v'=2)$ dissociation limit. The shift of the turn-on of the continuum from the $I^{35}Cl$ B−X, 2−0 band origin at 17 664.08 cm^{-1} represents the binding energy of the *o*-$H_2\cdots I^{35}Cl(X,v''=0)$ complex involved in the transition, 186.4(3) cm^{-1}. Because the intensity of this signal tracks with the intensity of the higher energy features, this continuum corresponds to transitions of the conformer with C_{2v} symmetry. The continuum signal with a turn-on at 17 820.9 cm^{-1} is associated with transitions of the *p*-$H_2\cdots I^{35}Cl(X,v''=0)$ complex with C_{2v} symmetry, and a binding energy of 156.8(1.3) cm^{-1} is determined.

Because no bound-free signals are observed that are associated with the ground-state conformer with an asymmetric geometry, we estimate the binding energy in a manner similar to that utilized previously for T-shaped rare gas−dihalogen complexes.[25] In this method, we rely on the anharmonicity of the ICl(A) potential and determine when the $\Delta v = -1$ vibrational predissociation channels for the *o,p*-$H_2\cdots I^{35}Cl(A,v')$ complexes close to bracket the binding energy of the excited-state complexes. From the spectral shift of the complex features from the monomer band origin, we could then determine the ground-state binding energy of the asymmetric conformers.

Figure 4 contains action spectra acquired by scanning an excitation laser throughout different ICl A−X, v'−0 regions with the probe laser fixed in wavelength to detect ICl(A,v'−1) products. Panel a shows the spectrum obtained by scanning the excitation laser through the ICl A−X, 21−0 region with the probe laser fixed on the $I^{35}Cl$ β−A, 6−20 transition. In addition to the $I^{35}Cl(A,v'=21)$ and $He\cdots I^{35}Cl(A,v'=21)$ features that are marked with an asterisk and dagger, respectively, in the figure, *o*- and *p*-$H_2\cdots I^{35}Cl(A,v'=21)$ features are observed. The *o*-$H_2\cdots I^{35}Cl(A,v'=21)$ feature occurs at a lower transition energy than the *p*-$H_2\cdots I^{35}Cl(A,v'=21)$ feature, contrary to what was observed in the ICl B−X, 3−0 region. However, both features are present, implying that the $\Delta v = -1$ vibrational predissociation channel is open for both of the excited-state complexes. Panel b shows an analogous action spectrum for the ICl A−X, 22−0 region. Here, the $\Delta v = -1$ vibrational predissociation channel is open for the *p*-$H_2\cdots I^{35}Cl(A,v'=22)$ complex, but it closes for *o*-$H_2\cdots I^{35}Cl(A,v'=22)$. In the same manner, it is seen in panels c and d that the $\Delta v = -1$ vibrational predissociation channel is open for *p*-$H_2\cdots I^{35}Cl(A,v'=23)$, but closed for *p*-$H_2\cdots I^{35}Cl(A,v'=24)$. Considering the transition energies to the $I^{35}Cl(A,v')$ levels,[26] the excited-state binding energy, D_0', of the asymmetric *o*-$H_2\cdots I^{35}Cl(A,v'=21)$ complex is <82.9 cm^{-1}, and that of the asymmetric *o*-$H_2\cdots I^{35}Cl(A,v'=22)$ complex is >74.9 cm^{-1}. The ground-state binding energy, D_0'', of the asymmetric *o*-$H_2\cdots I^{35}Cl(X,v''=0)$ conformer is then $82.8 \le D_0'' \le 89.6$ cm^{-1}. Likewise, for the asymmetric *p*-$H_2\cdots I^{35}Cl(X,v''=0)$ conformer we find $70. \le D_0'' \le 77.9$ cm^{-1}. The binding energies for the observed asymmetric and C_{2v} symmetric $H_2\cdots I^{35}Cl(X,v''=0)$, $H_2\cdots I^{35}Cl(B,v'=3)$, and $H_2\cdots I^{35}Cl(A,v'=23)$ complexes are listed in Table 3.

TABLE 2: Rigid-Rotor Parameters (cm^{-1}) for the Asymmetric *o*-$H_2\cdots$ICl B−X, 3−0 Rovibronic Band

ν_0	17840.75		
A''	0.346	A'	0.304
B''	0.113	B'	0.080
C''	0.091	C'	0.069

TABLE 3: Binding Energies (cm^{-1}) for the Different *o*-$H_2\cdots I^{35}Cl$ and *p*-$H_2\cdots I^{35}Cl$ Conformers and States

	C_{2v} conformer		asymmetric conformer	
	o-H_2	*p*-H_2	*o*-H_2	*p*-H_2
$I^{35}Cl(X,v''=0)$	186.4(3)	156.8(1.3)	$82.8 \le D_0'' \le 89.6$	$70. \le D_0'' \le 77.9$
ICl(A,v′=23)			$73.7 \le D_0' \le 80.5$	$59.2 \le D_0' \le 67.1$
ICl(B,v′=3)			$69.5 \le D_0' \le 76.3$	$59.4 \le D_0' \le 67.3$

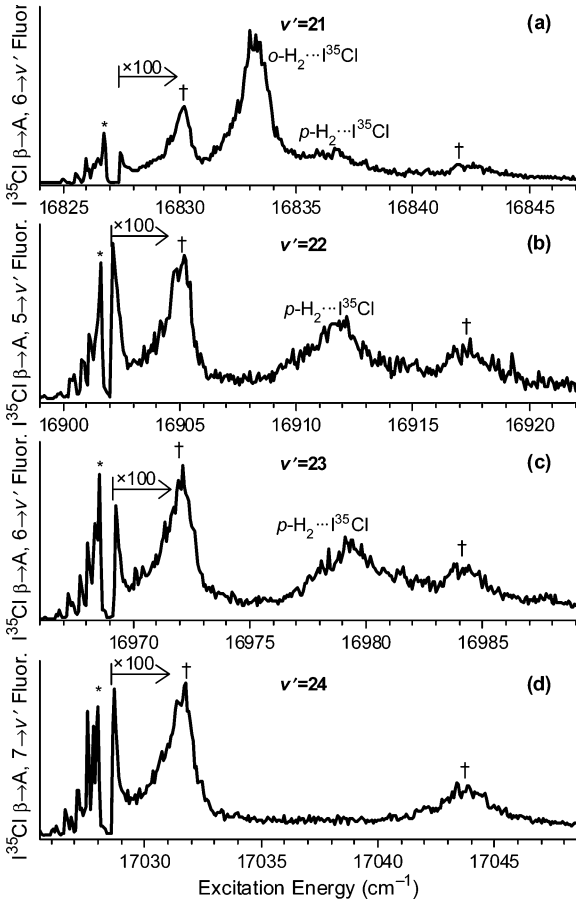

Figure 4. $\Delta v = -1$ action spectra recorded in the $I^{35}Cl$ A−X, $v'-0$ spectral region. Panels a and b illustrate the closing of the $\Delta v = -1$ vibrational predissociation channel for *o*-$H_2\cdots I^{35}Cl(A,v')$, and (c) and (d) illustrate the same effect for *p*-$H_2\cdots I^{35}Cl(A,v')$. From these channel closings, the ground-state binding energy of the more weakly bound, asymmetric *o,p*-$H_2\cdots I^{35}Cl(X,v''=0)$ conformer can be determined. Asterisks and daggers indicate $I^{35}Cl$ and $He\cdots I^{35}Cl$ features, respectively.

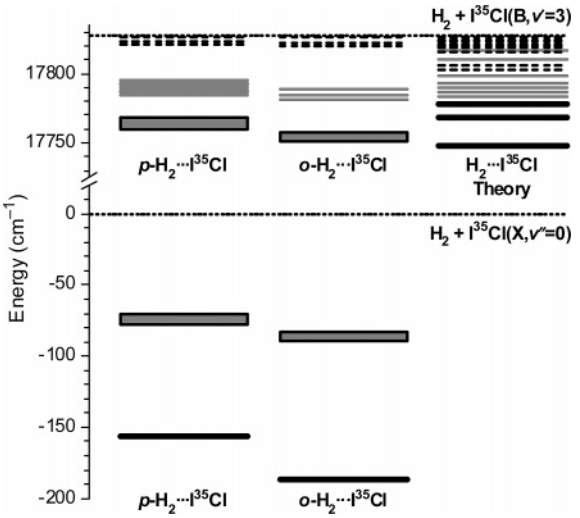

Figure 5. Energy level diagram of the bound *o,p*-$H_2\cdots I^{35}Cl(X,v''=0)$ and *o,p*-$H_2\cdots I^{35}Cl(B,v'=3)$ levels observed. The black lines in the ground state correspond to the energies of the C_{2v} symmetric conformers. The gray boxes in both the ground and excited states are the energies of the asymmetric conformers with the breadth representing the uncertainty. The gray lines in the excited state are accessed by transitions of the C_{2v} conformer and are delocalized in the angular coordinate. The dashed lines are also accessed by transitions of the C_{2v} conformer but are believed to have intermolecular stretching on the basis of comparison with calculations. The calculated excited-state levels, $n' = 0-19$, used in part to make the assignments are shown on the right.

The ability to observe transitions associated with both the asymmetric and C_{2v} symmetric conformers even though the binding energies are significantly different indicates that the complexes are not in thermal equilibrium when a carrier gas consisting of 5% *n*-H_2 in He is used. In contrast, we only observe transitions of the C_{2v} conformer at higher H_2 gas concentrations. This suggests that at the lower H_2 concentrations, the populations of the conformers are kinetically trapped in the supersonic expansion, and additional $H_2/H_2\cdots ICl(X,v''=0)$ collisions are necessary for further cooling of the complexes down to the most strongly bound C_{2v} symmetric conformer.[16,27]

E. Excited-State Assignments. The above results indicate that the spectroscopic features at 17 841, 17 968, 17 975, and 18 006 cm^{-1} in the ICl B−X, 3−0 region are attributable to transitions of the *o*-$H_2\cdots I^{35}Cl$ ground-state complex. Furthermore, the feature at 17 841 cm^{-1} corresponds to a transition of the conformer with an asymmetric structure, whereas the others arise from transitions of the C_{2v} symmetric ground-state conformer. The binding energies of the ground-state conformers permit the energies of the excited-state levels relative to the *o*-H_2 + $I^{35}Cl(B,v'=3)$ dissociation limit to be determined. The lowest-lying *o*-$H_2\cdots I^{35}Cl(B,v'=3)$ level with no intermolecular vibrational excitation, $n' = 0$, lies between −69.5 and −76.3 cm^{-1} relative to the dissociation limit. The features accessed by transitions of the C_{2v} conformer, at 17 968 and 17 975 cm^{-1}, have congested contours similar to that shown in Figure 3c and probably consist of transitions to multiple intermolecular vibrational levels. These levels are at −46 and −39 cm^{-1} with respect to the asymptote. The excited-state level associated with the higher energy feature at 18 006 cm^{-1} is at −8 cm^{-1} and is also accessed by transitions of the C_{2v} conformer.

The theoretical calculations of the energies and probability amplitudes of the excited-state intermolecular vibrational levels, evaluated using the model B-state potential, are used to tentatively assign the observed intermolecular vibrational levels and to gain insights into the intermolecular excitation within these levels. The energies of the bound intermolecular vibrational levels, $n' = 0-19$, are shown in the right column of Figure 5. The probability amplitudes shown in Figure 6 indicate that the lowest three vibrational levels, $n' = 0-2$, are localized in the well near $\theta = 100°$, and with increasing n' a bending excitation of the H_2 moiety about the ICl is apparent. Transitions of the ground-state, asymmetric *o*-$H_2\cdots I^{35}Cl(X,v''=0)$ conformer most likely access the $n' = 0$ level on the basis of favorable Franck−Condon overlap. The probability amplitudes of the next higher levels, $n' = 3-7$, as well as $n' = 10$ and 12, are delocalized in the angular coordinate. On the basis of the large

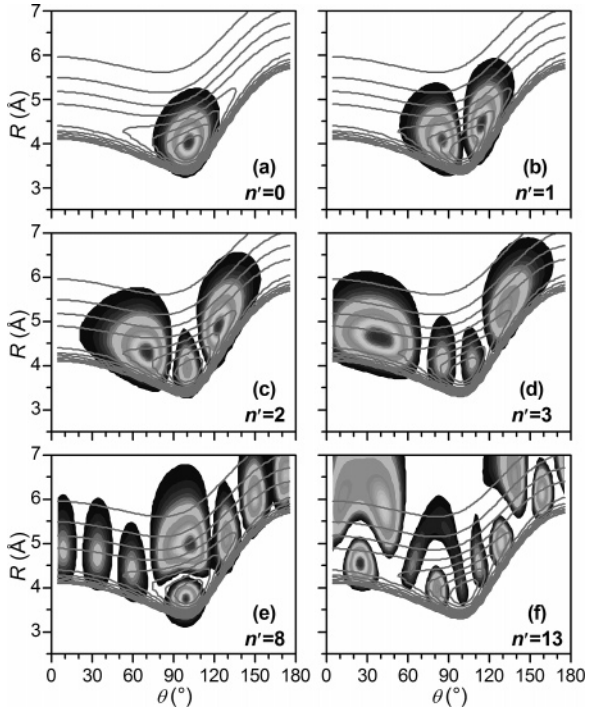

Figure 6. Probability amplitudes for numerous $H_2\cdots ICl(B,v'=3)$ intermolecular vibrational levels, n', superimposed on the potential energy surface, gray lines, approximated by scaling a He + ICl(B,v'=3) potential.[17]

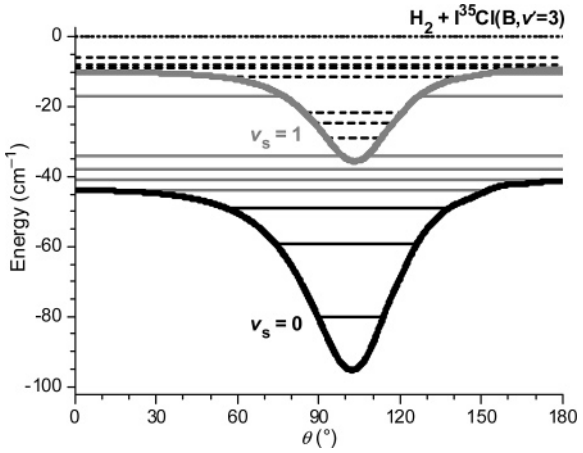

Figure 7. Adiabatic intermolecular potential energy curves for H_2 + ICl(B,v'=3) plotted as a function of θ, the angle between the ICl bond and the vector that connects the H_2 and ICl centers of mass. The v_s = 0 and v_s = 1 curves are those obtained by averaging over the radial coordinate without and with one quantum of intermolecular stretching excitation. The black, gray, and dashed horizontal lines represent the intermolecular levels that are localized, that are delocalized in the angular coordinate, and that exhibit intermolecular stretching excitation, respectively.

probability amplitude in the linear region, $\theta = 0°$, for the $n' = 3-5$ levels, the transitions from the C_{2v} symmetric o-$H_2\cdots I^{35}Cl(X,v''=0)$ conformer probably access these levels. The small energy spacing between these levels suggests that indeed there are many intermolecular vibrational levels accessed within each observed band.

The probability amplitudes indicate that there are bound levels with intermolecular stretching motion, as indicated by a node in the radial coordinate. The rotational contour analysis of the asymmetric band indicates a small change in geometry between the ground-state, asymmetric o-$H_2\cdots I^{35}Cl(X,v''=0)$ conformer and the lowest intermolecular vibrational energy level, for which the probability amplitude is shown in Figure 6a. When the radial node of the probability amplitude is localized in the well near 100°, as with the $n' = 8$ level shown in Figure 6e, it is presumed that the Franck−Condon factor will be small and transitions to these levels will most likely not be observed. The $n' = 13-15$ probability amplitudes again exhibit appreciable amplitude in the linear, $\theta = 0°$, region. These levels resemble delocalized states with intermolecular stretching excitation. As illustrated in Figure 6f for the $n' = 13$ level, the radial node for these levels is at significantly large R. Thus, there is most likely appreciable Franck−Condon overlap between these levels and the ground-state, symmetric C_{2v} $H_2\cdots I^{35}Cl(X,v''=0)$ conformer.

The excited-state levels accessed by transitions of the ground-state, asymmetric and C_{2v} symmetric $H_2\cdots ICl(X,v''=0)$ conformers are easily recognized by considering the angular-dependent, adiabatic potentials. The θ-dependent adiabatic potential curves obtained by averaging over the intermolecular distance coordinate, R, are plotted in Figure 7. The lower curve represents the adiabat associated with no nodes along R, v_s = 0, and the higher energy curve was calculated for one node along R, indicating $v_s = 1$. The $v_s = 1$ adiabat is at sufficiently high energy that it is embedded in $v_s = 0$ states that have nearly free-rotor character. Additionally, the first few states in this adiabat have radial nodes that are localized in the minimum. Once the radial nodes in the $v_s = 1$ states access the regions near $\theta = 0°$, they can be accessed by transitions of the ground-state, C_{2v} symmetric conformer.

The experimentally observed o-$H_2\cdots I^{35}Cl(B,v'=3)$ and p-$H_2\cdots I^{35}Cl(B,v'=3)$ levels are shown in the energy level diagram in Figure 5 with the line types indicating the type of vibrational excitation for each level, black solid-localized in the well, gray solid-delocalized, black dashed-delocalized with stretching excitation. The assignments of n' for the low-lying levels are most likely accurate, but on the basis of the simplicity of the excited-state potential, accurate assignments are not made for higher levels. Rather, the aim here is to illustrate the types of states that are being accessed.

5. Discussion

The only other hydrogen molecule−dihalogen molecule complex that has been reported is $H_2\cdots I_2$.[7] Only one conformer was reported for $H_2\cdots I_2$, and the spectrum strongly resembles the lower energy feature observed for the H_2 + $I^{35}Cl$ system. Although the authors did not explicitly report the geometry of the complex, similarities of the $H_2\cdots I_2$ spectrum to rare gas−dihalogen spectra suggest that the H_2 moiety is localized in the T-shaped well; i.e., the vector connecting the centers of mass of the constituent molecules is orthogonal to the dihalogen bond. Nevertheless, other hydrogen-containing complexes have been studied in much greater detail, and insights into the nature of the H_2 + ICl interactions can be deduced from them. For instance, Nesbitt and co-workers studied the $H_2\cdots HF$ and $H_2\cdots HCl$ complexes in the infrared using a slit jet expansion.[9,10] They reported preferred geometries with C_{2v} symmetry in both cases, with the H_2 subunit positioned at the hydrogen end of the hydrogen halide. Lester and co-workers reported a similar C_{2v} geometry for the $H_2\cdots H-O$ complex using electronic spectroscopy, and theoretical calculations were found to be consistent with their proposed geometry.[11] More recently, however, the Heaven group reported theoretical and experimental results on the $H_2\cdots CN$ and $H_2\cdots NH$ systems and argued that those complexes are linear, with the H_2 moiety at the nitrogen atom end in each case, $H-H\cdots N-C$ and $H-H\cdots N-H$.[12−14] Although there is a minimum in the potential in the C_{2v}

$H_2\cdots H-N$ and $H_2\cdots C-N$ orientations, the global minimum occurs in the linear orientation. The authors convincingly argue that the relatively small quadrupole moment of CN and NH compared to OH and HF enhance the stability of the linear conformer over that of the C_{2v} conformer because quadrupole−quadrupole interactions are repulsive for linear geometries but attractive for T-shaped structures.[14]

Though we are unaware of any experimental values for the quadrupole moment of ICl, numerous theoretical methods predict that it will be greater than 2 au, which is significantly greater than the quadrupole moment for both OH and HF, 1.39 and 1.75 au, respectively.[28−31] If we invoke Heaven's reasoning to the present case, then it seems likely that the more strongly bound $H_2\cdots I^{35}Cl(X,v''=0)$ conformer has a C_{2v} geometry with the H_2 moiety at the iodine side of the dihalogen with its bond axis positioned orthogonally to the dihalogen axis. This geometry optimizes the overlap between the toroid of negative charge around the H_2 bond and the positive charge at the iodine end of ICl. As discussed in the Results, the rotational contours of the less strongly bound conformer imply an asymmetric geometry with the H_2 molecule oriented perpendicularly to the I−Cl bond axis. The precise positioning of each of the hydrogen atoms and the direction of rotation are still unknown, and it will most likely require a more accurate PES, calculated for H_2−ICl and including more than two internal degrees of freedom, to gain additional insights. Nevertheless, the electrostatic interactions present for the C_{2v} conformer will not be present for the asymmetric conformer, and it should therefore be less strongly bound.

We have measured the binding energies of both the asymmetric and C_{2v} symmetric $H_2\cdots I^{35}Cl(X,v''=0)$ conformers; the C_{2v} conformer is significantly more strongly bound than the asymmetric conformer, by $\approx$100 cm^{-1}. This large difference is in significant contrast to the nearly isoenergetic linear and T-shaped Rg···XY complexes, where the binding energies of the linear conformers are $\approx$0−15 cm^{-1} larger than the T-shaped conformers.[3,5,6,17,24] We propose that these differences in binding energies are direct consequences of the important roles that electrostatic interactions play in the stabilization of the *o*,*p*-$H_2\cdots I^{35}Cl(X,v''=0)$ complexes.

We also determined that the *o*-$H_2\cdots I^{35}Cl$ levels are more strongly bound than the *p*-$H_2\cdots I^{35}Cl$ levels in both the ground and excited electronic states. This is consistent with the observations of the Heaven, Lester, and Nesbitt groups and has been attributed to the symmetry of the H_2 wavefunction, with the node in the $j = 1$ state serving to enhance the quadrupolar interactions of H_2.[9−11,13,14] We note that the differences in binding energies are not drastic with $D_0'' = 186.4(3)$ versus 157.0(1.3) cm^{-1}, or a 19% enhancement for the C_{2v} *o*-$H_2\cdots I^{35}Cl(X,v''=0)$ complex over that of the *p*-$H_2\cdots I^{35}Cl(X,v''=0)$ complex. Nevertheless, the differences in binding energies is substantial enough so that the *o*,*p*-$H_2\cdots I^{35}Cl$ features are not observed in the 3:1 ratio expected for *n*-H_2. When the source conditions are changed, however, the relative intensities of the *o*,*p*-$H_2\cdots I^{35}Cl$ features can be altered, as exhibited in Figure 2. We hypothesize that the reason we see changing intensities of the *o*-$H_2\cdots I^{35}Cl$ and *p*-$H_2\cdots I^{35}Cl$ populations arises from an exchange mechanism where *p*-H_2 molecules are replaced by the more abundant and more strongly interacting *o*-H_2 molecules with collisions along the expansion. Exchange reactions most likely result in conversion of the higher energy asymmetric $H_2\cdots ICl(X,v''=0)$ conformers to the more stable C_{2v} symmetric conformers. The net result, then, would be that the most stable C_{2v} *o*-$H_2\cdots ICl(X,v''=0)$ species will tend to grow in relative to the populations of the other, more weakly bound species observed in the expansion as the number of H_2 + ICl collisions increases.

The interactions in the excited-state potentials of the H_2 + $ICl(B,v')$ and Rg + $XY(B,v')$ systems are quite similar, with the H_2 and Rg moieties localized in a minimum positioned orthogonally to the I−Cl bond axis. There appears to be only one minimum in the excited-state potential, and the features of the rovibronic spectrum are surprisingly insensitive to the detailed topology of the B-state surface.[6] The transitions of the ground-state, asymmetric $H_2\cdots ICl(X,v''=0)$ and T-shaped $Rg\cdots ICl(X,v''=0)$ conformers access localized levels in the excited state with nearly identical geometries. In contrast, the C_{2v} symmetric $H_2\cdots ICl(X,v''=0)$ and linear $Rg\cdots ICl(X,v''=0)$ conformers access levels that are delocalized in the angular coordinate. Last, excited-state levels with intermolecular stretching excitation are only accessed by transitions of the ground-state, C_{2v} symmetric conformer. This is most likely because of the large increase in internuclear separation induced with electronic excitation in the complexes in the linear orientation.

The results reported here characterizing the *o*,*p*-H_2 + $I^{35,37}Cl$ ground- and excited-state interactions should be helpful in clarifying the role that electrostatic interactions play in the stabilization of weakly bound van der Waals complexes. In particular, the ground-state binding energies should serve as excellent targets for potentials calculated by applying advanced methodology to determine four-atom interactions. It would be interesting to compare and contrast these results to those for different conformers of a homonuclear $H_2\cdots XY$ complex, where there is no dipole, to further elucidate the role of dipole−quadrupole interactions in these complexes. Comparisons of the *o*,*p*-H_2 + $I^{35,37}Cl$ ground- and excited-state interactions with the corresponding D_2 + $I^{35,37}Cl$ interactions would also aid in characterizing the *o*,*p*-H_2 + $I^{35,37}Cl$ ground- and excited-state PESs in greater detail.

Acknowledgment. R.A.L. is indebted to the David and Lucile Packard Foundation for a Fellowship in Science and Engineering and to the National Science Foundation for a CAREER Award, CHE-0346745. R.A.L. thanks the donors of The Petroleum Research Fund, administered by the American Chemical Society, for partial support of this research. A.B.M. acknowledges the National Science Foundation CHE-0515627. We thank M. C. Heaven for valuable discussions and are indebted to B. J. McCall for experimental assistance with the preparation of the high-purity *p*-H_2.

References and Notes

(1) Bradke, M. D.; Loomis, R. A. *J. Chem. Phys.* **2003**, *118*, 7233.

(2) Boucher, D. S.; Darr, J. P.; Bradke, M. D.; Loomis, R. A.; McCoy, A. B. *Phys. Chem. Chem. Phys.* **2004**, *6*, 5275.

(3) Strasfeld, D. B.; Darr, J. P.; Loomis, R. A. *Chem. Phys. Lett.* **2004**, *397*, 116.

(4) Boucher, D. S.; Strasfeld, D. B.; Loomis, R. A.; Herbert, J. M.; Ray, S. E.; McCoy, A. B. *J. Chem. Phys.* **2005**, *123*, 104312/1.

(5) Darr, J. P.; Glennon, J. J.; Loomis, R. A. *J. Chem. Phys.* **2005**, *122*, 131101.

(6) Ray, S. E.; McCoy, A. B.; Glennon, J. J.; Darr, J. P.; Fesser, E. J.; Lancaster, J. R.; Loomis, R. A. *J. Chem. Phys.* **2006**, *125*, 164314.

(7) Kenny, J. E.; Russell, T. D.; Levy, D. H. *J. Chem. Phys.* **1980**, *73*, 3607.

(8) Darr, J. P.; Crowther, A. C.; Loomis, R. A. *Chem. Phys. Lett.* **2003**, *378*, 359.

(9) Lovejoy, C. M.; Nelson, D. D., J.; Nesbitt, D. J. *J. Chem. Phys.* **1987**, *87*, 5621.

(10) Anderson, D. T.; Schuder, M.; Nesbitt, D. J. *Chem. Phys.* **1998**, *239*, 253.

(11) Loomis, R. A.; Lester, M. I. *Annu. Rev. Phys. Chem.* **1997**, *48*, 643.

(12) Fawzy, W. M.; Kerenskaya, G.; Heaven, M. C. *J. Chem. Phys.* **2005**, *122*, 144318.

(13) Chen, Y.; Heaven, M. C. *J. Chem. Phys.* **1998**, *109*, 5171.

(14) Kaledin, A. L.; Heaven, M. C.; Bowman, J. M. *J. Chem. Phys.* **1999**, *110*, 10380.

(15) Chen, Y.; Heaven, M. C. *J. Chem. Phys.* **2000**, *112*, 7416.

(16) Boucher, D. S.; Bradke, M. D.; Darr, J. P.; Loomis, R. A. *J. Phys. Chem. A* **2003**, *107*, 6901.

(17) McCoy, A. B.; Darr, J. P.; Boucher, D. S.; Winter, P. R.; Bradke, M. D.; Loomis, R. A. *J. Chem. Phys.* **2004**, *120*, 2677.

(18) Waterland, R. L.; Skene, J. M.; Lester, M. I. *J. Chem. Phys.* **1988**, *89*, 7277.

(19) Darr, J. P.; Ray, S. E.; McCoy, A. B.; Loomis, R. A. Manuscript in preparation.

(20) Skene, J. M.; Lester, M. I. *Chem. Phys. Lett.* **1985**, *116*, 93.

(21) Skene, J. M. The spectroscopy and dynamics of iodine monochloride-rare gas van der Waals compelxes. Ph.D. Thesis, University of Pennsylvania, 1988.

(22) Cline, J. I.; Sivakumar, N.; Evard, D. D.; Bieler, C. R.; Reid, B. P.; Halberstadt, N.; Hair, S. R.; Janda, K. C. *J. Chem. Phys.* **1989**, *90*, 2605.

(23) Plusquellic, D. F. (2002). *User Guide to the Jb95 Spectral Fitting Program* (v2.00.3). Available online http://physics.nist.gov/jb95 [2007, July 11]. National Institute of Standards and Technology, Gaithersburg, MD.

(24) Darr, J. P.; Loomis, R. A.; McCoy, A. B. *J. Chem. Phys.* **2005**, *122*, 044318.

(25) Blazy, J. A.; DeKoven, B. M.; Russell, T. D.; Levy, D. H. *J. Chem. Phys.* **1980**, *72*, 2439.

(26) Coxon, J. A.; Gordon, R. M.; Wickramaaratchi, M. A. *J. Mol. Spectrosc.* **1980**, *79*, 363.

(27) Bastida, A.; Zúñiga, J.; Requena, A.; Miguel, B.; Beswick, J. A.; Vigué, J.; Halberstadt, N. *J. Chem. Phys.* **2002**, *116*, 1944.

(28) de Leeuw, F. H.; Dymanus, A. *J. Mol. Spectrosc.* **1973**, *48*, 427.

(29) Esposti, A. D.; Werner, H. *J. Chem. Phys.* **1990**, *93*, 3351.

(30) Sadlej, A. J. *J. Chem. Phys.* **1992**, *96*, 2048.

(31) de Jong, W. A.; Styszynski, J.; Visscher, L.; Nieuwpoort, W. C. *J. Chem. Phys.* **1998**, *108*, 51775184.